Deep learning-based noise reduction preserves quantitative MRI biomarkers in patients with brain tumors

Geoffroy Pouliquen, Clément Debacker, Sylvain Charron, Alexandre Roux, Corentin Provost, Joseph Benzakoun, Wolter de Graaf, Valentin Prevost, Johan Pallud, Catherine Oppenheim

Deep learning-based noise reduction preserves quantitative MRI biomarkers in patients with brain tumors

Geoffroy Pouliquen[a,b$], Clément Debacker[a,b$], Sylvain Charron[a,b], Alexandre Roux[b,c], Corentin Provost[a,b], Joseph Benzakoun[a,b], Wolter de Graaf[d], Valentin Prevost[e], Johan Pallud[b,c], Catherine Oppenheim[a,b*]

[$]*Equal contribution.*

[a]Imaging department, GHU-Paris Psychiatrie et Neurosciences, Hôpital Sainte Anne, F-75014 Paris, France.

[b]Université Paris Cité, Institute of Psychiatry and Neuroscience (IPNP), INSERM U1266, 75014 Paris, France.

[c]Neurosurgery department, GHU-Paris Psychiatrie et Neurosciences, Hôpital Sainte Anne, F-75014 Paris, France.

[d]Canon Medical Systems Europe B.V., 2718 RP, The Netherlands

[e]Canon Medical Systems Corporation, Otawara, Japan

*Corresponding author: **c.oppenheim@ghu-paris.fr**

Tel: +33145658242

DEEP LEARNING-BASED NOISE REDUCTION PRESERVES QUANTITATIVE MRI BIOMARKERS IN PATIENTS WITH BRAIN TUMORS

Abstract

The use of relaxometry and Diffusion-Tensor Imaging sequences for brain tumor assessment is limited by their long acquisition time. We aim to **test the effect of** a denoising algorithm based on a Deep Learning Reconstruction (DLR) technique on quantitative MRI parameters while reducing scan time. In 22 consecutive patients with brain tumors, DLR applied to fast and noisy MR sequences **preserves the mean values of quantitative parameters** (Fractional anisotropy, mean Diffusivity, T1 and T2-relaxation time) and **produces maps with higher structural similarity** compared to long duration sequences. This could promote wider use of these biomarkers in clinical setting.

Abbreviations

AiCE: Advanced intelligent Clear IQ-Engine

DLR: denoising approach using Deep Learning-based Reconstruction

DTI: Diffusion-Tensor Imaging

FA: Fractional Anisotropy

FLAIR: Fluid-Attenuated Inversion Recovery

MAD: Mean Absolute Deviation

MD: Mean Diffusivity

MPRAGE: Magnetization Prepared Rapid Acquisition Gradient Echo

MP2RAGE: Magnetization Prepared 2 Rapid Acquisition Gradient Echoes

MRI: Magnetic Resonance Imaging

NAQ: Number of Acquisitions

RT: Relaxation Time

ROI: Region-Of-Interest

SD: Standard Deviation

SSIM: Structural Similarity Index Measure

Keywords

Deep learning

Denoising

Relaxometry

Diffusion tensor imaging

Magnetic Resonance Imaging

Brain tumors

Introduction

Multiparametric MRI is used to characterize brain tumors.[1,2] Advanced techniques, like relaxometry and Diffusion-Tensor Imaging (DTI), provide quantitative biomarkers that may help brain tumor characterization, gradation, and molecular subtype **classification.**[1,3–5] Moreover, T2-mapping may improve the delineation of the actual tumor margins beyond maximal visible T2/FLAIR signal changes in diffuse gliomas.[6] However, the additional acquisition time reduces the acceptance of relaxometry and DTI in routine.

Exceptional progress have been achieved in artificial intelligence and its application to neuroimaging, holding promises for optimization of image acquisition.[7] Denoising using deep learning algorithms during reconstruction improves image quality or compensates for the degradation induced by acquisition acceleration.[8–14] **The denoising approach using Deep Learning-Reconstruction (DLR), marketed by various manufacturers, is based on the detection of the noise's profile to remove it. DLR commercialized as Advanced Intelligent Clear IQ-Engine (AiCE), can potentially be applied to various MR sequences as it is independent of the scan type.**[15] However, its effect on multiparametric quantitative MRI is uncertain, since it has been trained on conventional T1 and T2-weighted images in healthy volunteers. **In phantoms and healthy controls, DLR drastically reduced image noise and generated MR brain image (FLAIR, T2 and 3D-T1) with sufficient quality to evaluate fine anatomic details in short acquisition time.**[15] DLR was **also** shown to provide reliable diffusion parameters while reducing acquisition time in patients without active brain lesions or with prostate cancer.[16,17] The benefit on other metrics and its feasibility in patients with brain tumors are unknown.

We hypothesized that DLR would preserve quantitative measurements. We therefore compared mean values of fractional anisotropy [FA], mean diffusivity [MD], T1 and T2-Relaxation Times [RT] derived from fast and noisy MR sequences denoised

with DLR to those of longer sequences without DLR, used as a reference, in patients with brain tumors. Compared to a short non-DLR sequence, we also verified that DLR reduced the standard deviation (SD) of MR parameters and had higher structural similarity index measure (SSIM) with respect to the reference sequence.

Material and Methods

Patients

This prospective study was approved by the ethical committee (NCT05618990) and patients gave their written informed consent. From April to June 2021, 22 patients with a known or suspected brain tumor were included (Table 1). All were naïve of any oncological treatment. The final diagnosis was based on histomolecular analyses when available, or on all clinical and imaging information.

MRI acquisition

Before inclusion, all patients had a clinical 3T MRI (GE Healthcare, MR 750) using a standardized brain tumor protocol. For this study, additional scans were performed on a 3T MRI (Vantage Galan 3T/XGO; Canon Medical Systems) with a 32-channel head coil (Table 2): 3D T1-magnetization prepared rapid acquisition gradient echo (MPRAGE) for intra-subject registration; DTI using a single-shot echo-planar imaging sequence with gradients applied in 30 directions and phase-encode blip with opposite polarity for susceptibility-induced distortions correction; 3D T1-magnetization prepared 2 rapid acquisition gradient echoes (MP2RAGE) to generate T1-RT maps; 2D T2-fast spin echo sequence to generate T2-

RT maps. Each quantitative sequences were acquired twice**: number of acquisitions equal to one (NAQ1, duration≈3min) and equal to three (NAQ3, duration≈9min). NAQ3 served as ground truth data for the mean values of quantitative parameters. All sequences were acquired** without reconstruction filter.

Denoising

NAQ1 data were reconstructed using the vendor-supplied DLR algorithm (AiCE, Canon Medical Systems) and termed DLR-NAQ1. Briefly, DLR is a convolutional neural network aimed for denoising after learning various noise characteristics using training pairs of different noise level images and the corresponding ground-truth images from healthy volunteers. Separation of the data in different frequency components using a discrete cosin transform maintains the image contrast regardless of the scan type during the process.[15,16]

The DLR tools allow to set **a** denoising level with a blending factor and an edge enhancement step. The latter, based on an "unsharp mask", was not applied to minimize the risk of modifying quantitative values at image boundaries. The denoising level was gradually increased and final settings determined visually, based on the delineation of the basal ganglia and the contrast between cortex and white matter.[15,16] The blending factor weighted the denoised image with the raw one, aiming to obtain a final output matching clinical preferences. The DLR settings are described in Table 2.

Data preparation

T1 and T2-RT maps were generated using the NOVA+ tool (OLEA SPHERE 3.0). Data were post-processed using FMRIB Software Library

(https://fsl.fmrib.ox.ac.uk/fsl/fslwiki).[18] From the pairs of DTI data collected with lrsed phase-encode blips, the susceptibility-induced off-resonance field was estimated and the two images were combined into a single corrected one using *topup*. Outputs were corrected for eddy current and motion-distortions using *eddy*. FA and MD were computed using the *dtifit* command. The parametric maps (FA, MD, T1 and T2-RT maps) were co-registered onto the 3D-anatomical scan of each patient using a 3D rigid-registration via *FLIRT*.

Quantitative biomarkers

Using Mango (http://ric.uthscsa.edu/mango/), regions-of-interest (ROIs) were positioned on the anatomical images in the following normal brain areas: cortex and white matter of frontal and parietal lobes as well as the putamen. Spherical ROIs (mean, 85 mm^3) were placed respectively in the enhanced or central portion of the tumor (when enhancement was lacking) and the peritumoral edema or at the periphery of the lesion when homogeneous. ROIs were copied on the co-registered parametric maps to extract mean ± SD of FA, MD, T1 and T2-RT values for NAQ1, DLR-NAQ1 and NAQ3 images.

Denoising performance

The SSIM index shows the similarity of signal intensity, contrast and structure of each local region, to the reference NAQ3 maps. If denoising is efficient, SSIM increases indicating that the NAQ1-DLR maps share more similarity with the reference NAQ3 than NAQ1. Hence, we computed SSIM with respect to NAQ3 reference for NAQ1 and DLR-NAQ1 on each map.

Statistical analysis

The effect of the three acquisition-reconstruction methods on the mean and SD of quantitative MR parameters across ROI locations was assessed using a factorial design with repeated measures. Mean and SD for FA, MD, T1 and T2-RT were considered independent for the analyses. Since the mean and SD were not normally distributed, we performed an aligned rank transformation, then fitted a multilevel regression model to account for within-subject repetition.[19,20] First, interaction between the two main factors (acquisition-reconstruction methods; ROI locations) and their main effect were determined. Relevant post-hoc analyses for **significant** main effects were performed using pairwise comparisons with Hommel correction.[21] **SSIM were compared using Wilcoxon signed-rank test**. Results are expressed using median and mean absolute deviation (MAD). *P*-values were two-sided and $p<0.05$ considered significant.

Results

A total of 22 patients (11 women; mean age 56±14 years) were enrolled. Fig. 1 shows representative images calculated from NAQ1, DLR-NAQ1 and NAQ3.

The effect of DLR denoising on SSIM was significant for all maps, with DLR-NAQ1 being more similar to NAQ3 than NAQ1 (Table 3).

There was no significant interaction between acquisition-reconstruction methods and ROI location for both mean and SD of all studied parameters, except for FA. Leave-one out analysis identified the putamen ROI as driving this interaction. FA values were thus analysed separately for putamen and other ROIs.

The **main** effect of ROI locations on pooled acquisition-reconstruction methods was significant for mean of all quantitative parameters (**Supplementary Fig. S1**). They differed between brain areas, as expected.[22–24] For instance, mean FA were higher in healthy white matter than in cortex and T2-RT were higher in tumor than in healthy brain.

Results are presented for each parameter as median ± MAD (Table 4), with pooled ROIs across all locations (apart from FA in the putamen) to focus on the main effect of acquisition-reconstruction methods.

FA values **(Fig. 2-3)**

Mean values were significantly higher in NAQ1 than in DLR-NAQ1 or NAQ3 but did not differ between DLR-NAQ1 and NAQ3. SDs were significantly higher in NAQ1 than in DLR-NAQ1 or NAQ3 SD was significantly lower in DLR-NAQ1 than in NAQ3.

Putamen ROIs presented similar effects for mean FA, the interaction emerging from a wider difference between NAQ1 and DLR-NAQ1 or NAQ3. However, for putamen ROIs, SDs in NAQ1 were not significantly different than in DLR-NAQ1 but were higher than in NAQ3. SDs were not significantly different in DLR-NAQ1 compared to NAQ3.

MD values **(Fig. 4)**

Mean values were not significantly different between NAQ1, DLR-NAQ1 and NAQ3. SDs were significantly higher in NAQ1 compared with DLR-NAQ1 or NAQ3. SDs were significantly lower in DLR-NAQ1 compared to NAQ3.

T1-RT **(Fig. 5)**

Mean values were not significantly different between NAQ1, DLR-NAQ1 and NAQ3. SDs were significantly higher in NAQ1 compared with DLR-NAQ1 or NAQ3 but did not significantly differ between DLR-NAQ1 and NAQ3.

T2-RT **(Fig. 6)**

Mean values were not significantly different between NAQ1, DLR-NAQ1 and NAQ3. SDs were significantly higher in NAQ1 compared with DLR-NAQ1 or NAQ3 but did not significantly differ between DLR-NAQ1 and NAQ3.

Discussion

In a series of 22 consecutive patients with brain tumors, **DLR applied to fast and noisy quantitative MR sequences preserved mean values of parameters (FA, MD, T1 and T2-RT) as compared to long duration sequences.**

In line with others, we confirm that DLR does not have adverse effect on **the mean value of** MD[17,25] and expand this result to FA and relaxometry. **Our findings suggest that DLR applied to short sequences could replace long duration acquisitions, given the high similarity with the NAQ3 reference maps.**

As expected **denoising using DLR decreases SD of most parameters, compared to the same non-DLR short sequence. Regarding FA and MD, SDs were smaller in DLR-NAQ1 than in NAQ3. This unexpected finding might be explained by a stronger noise reduction using DLR than using increase signal average as done in NAQ3. It might also be due to increased motion artifacts with the longer NAQ3 images that were obtained**

after NAQ1. However, findings were consistent for all parameters, although sequences were always acquired in the same order, suggesting that motion artifacts did not play a major role. Overall, the SD reduction we observed reflects noise reduction and likely translates into an improvement of quantitative parameters. However, denoising could remove physiological variability and attenuate clinically relevant variations. This is unlikely because structural similarity to the NAQ3 reference was higher on quantitative maps after DLR denoising.

One could argue that a sequence with short duration without DLR could be sufficient to obtain clinical usable values. We, however, found higher FA values with the noisy NAQ1 sequence compared to those with DLR and the reference sequence, whereas MD values were similar. This is not unexpected given that the estimation of eigenvectors is function of signal-to-noise ratio: increasing $\lambda 1$ and concurrently decreasing $\lambda 3$ at low signal-to-noise ratio accounts for an upward FA bias. Conversely, as the biases in $\lambda 1$ and $\lambda 3$ offset each other, MD values remain stable.[26] The low signal-to-noise ratio in deep brain region with higher iron load and distant to the receiver coil might also explain the variability of FA in the putamen, requiring specific adjustments of the denoising level.[16] **Importantly, the effect of DLR could be greater when applied to noisier sequences than the ones understudy. Gradual undersampling of MR sequence will help determining to which extent duration can be reduced while preserving quantitative values with DLR.**

Our study has limitations. The study sample was small. **MRI data and DLR method were from a single vendor, precluding generalization. The denoising level was determined empirically so may not be optimal.** Further studies focused on a comprehensive compromise offered by DLR applied to quantitative MRI are needed.

DLR applied to fast quantitative MR sequences does not have an adverse effect on derived quantitative biomarkers in patients with brain tumors. In the context of the ever-

increasing throughput expectations of radiology departments, reduction of scan time can facilitate wider use of techniques that could help with tumor characterization, such as relaxometry and DTI.

Acknowledgement

We thank Anna Fayolle (research radiographer) for her major role in MR acquisition.

References

1.Kern M, Auer TA, Picht T, Misch M, Wiener E. T2 mapping of molecular subtypes of WHO grade II/III gliomas. BMC Neurol 2020;20:8. https://doi.org/10.1186/s12883-019-1590-1.

2.Bathla G, Dhruba DD, Soni N, Liu Y, Larson NB, Kassmeyer BA, et al. AI-based classification of three common malignant tumors in neuro-oncology: A multi-institutional comparison of machine learning and deep learning methods. J Neuroradiol 2023:S0150-9861(23)00237-7. https://doi.org/10.1016/j.neurad.2023.08.007.

3.Suh CH, Kim HS, Jung SC, Kim SJ. Diffusion-Weighted Imaging and Diffusion Tensor Imaging for Differentiating High-Grade Glioma from Solitary Brain Metastasis: A Systematic Review and Meta-Analysis. AJNR Am J Neuroradiol 2018;39:1208–14. https://doi.org/10.3174/ajnr.A5650.

4.Davanian F, Faeghi F, Shahzadi S, Farshidfar Z. Evaluation of Diffusion Anisotropy and Diffusion Shape in Grading of Glial Tumors. J Biomed Phys Eng 2019;9:459–64. https://doi.org/10.31661/jbpe.v0i0.513.

5.Guzman R, Altrichter S, El-Koussy M, Gralla J, Weis J, Barth A, et al. Contribution of the

apparent diffusion coefficient in perilesional edema for the assessment of brain tumors. J Neuroradiol 2008;35:224–9. https://doi.org/10.1016/j.neurad.2008.02.003.

6.Pallud J, Varlet P, Devaux B, Geha S, Badoual M, Deroulers C, et al. Diffuse low-grade oligodendrogliomas extend beyond MRI-defined abnormalities. Neurology 2010;74:1724–31. https://doi.org/10.1212/WNL.0b013e3181e04264.

7.Farrugia N. How feasible is end-to-end deep learning for clinical neuroimaging? J Neuroradiol 2022;49:399–400. https://doi.org/10.1016/j.neurad.2022.10.002.

8.Tajima T, Akai H, Yasaka K, Kunimatsu A, Yamashita Y, Akahane M, et al. Usefulness of deep learning-based noise reduction for 1.5 T MRI brain images. Clin Radiol 2023;78:e13–21. https://doi.org/10.1016/j.crad.2022.08.127.

9.Hu Y, Xu Y, Tian Q, Chen F, Shi X, Moran CJ, et al. RUN-UP: Accelerated multishot diffusion-weighted MRI reconstruction using an unrolled network with U-Net as priors. Magn Reson Med 2021;85:709–20. https://doi.org/10.1002/mrm.28446.

10.Kanemaru N, Takao H, Amemiya S, Abe O. The effect of a post-scan processing denoising system on image quality and morphometric analysis. J Neuroradiol 2022;49:205–12. https://doi.org/10.1016/j.neurad.2021.11.007.

11.Bischoff LM, Peeters JM, Weinhold L, Krausewitz P, Ellinger J, Katemann C, et al. Deep Learning Super-Resolution Reconstruction for Fast and Motion-Robust T2-weighted Prostate MRI. Radiology 2023;308:e230427. https://doi.org/10.1148/radiol.230427.

12.Moummad I, Jaudet C, Lechervy A, Valable S, Rabouter C, Soilihi, et al. The Impact of Resampling and Denoising Deep Learning Algorithms on Radiomics in Brain Metastases MRI. Cancers 2021;14. https://doi.org/10.3390/cancers14010036.

13.Cheng H, Vinci-Booher S, Wang J, Caron B, Wen Q, Newman S, et al. Denoising diffusion weighted imaging data using convolutional neural networks. PloS One 2022;17:e0274396. https://doi.org/10.1371/journal.pone.0274396.

14.Lee K-L, Kessler DA, Dezonie S, Chishaya W, Shepherd C, Carmo B, et al. Assessment of deep learning-based reconstruction on T2-weighted and diffusion-weighted prostate MRI image quality. Eur J Radiol 2023;166:111017. https://doi.org/10.1016/j.ejrad.2023.111017.

15.Kidoh M, Shinoda K, Kitajima M, Isogawa K, Nambu M, Uetani H, et al. Deep Learning Based Noise Reduction for Brain MR Imaging: Tests on Phantoms and Healthy Volunteers. Magn Reson Med Sci MRMS Off J Jpn Soc Magn Reson Med 2020;19:195–206. https://doi.org/10.2463/mrms.mp.2019-0018.

16.Sagawa H, Fushimi Y, Nakajima S, Fujimoto K, Miyake KK, Numamoto H, et al. Deep Learning-based Noise Reduction for Fast Volume Diffusion Tensor Imaging: Assessing the Noise Reduction Effect and Reliability of Diffusion Metrics. Magn Reson Med Sci 2020;20:450–6. https://doi.org/10.2463/mrms.tn.2020-0061.

17.Ueda T, Ohno Y, Yamamoto K, Murayama K, Ikedo M, Yui M, et al. Deep Learning Reconstruction of Diffusion-weighted MRI Improves Image Quality for Prostatic Imaging. Radiology 2022;303:373–81. https://doi.org/10.1148/radiol.204097.

18.Jenkinson M, Beckmann CF, Behrens TEJ, Woolrich MW, Smith SM. FSL. NeuroImage 2012;62:782–90. https://doi.org/10.1016/j.neuroimage.2011.09.015.

19.Wobbrock J, Findlater L, Gergle D, Higgins J. The Aligned Rank Transform for Nonparametric Factorial Analyses Using Only ANOVA Procedures. vol. 2011, 2011, p. 143–6. https://doi.org/10.1145/1978942.1978963.

20.Bates D, Mächler M, Bolker B, Walker S. Fitting Linear Mixed-Effects Models Using lme4. J Stat Softw 2015;67:1–48. https://doi.org/10.18637/jss.v067.i01.

21.Hommel G. A stagewise rejective multiple test procedure based on a modified Bonferroni test. Biometrika 1988;75:383–6. https://doi.org/10.1093/biomet/75.2.383.

22.Nakai K, Nawashiro H, Shima K, Kaji T. An analysis of T2 mapping on brain tumors. Acta Neurochir Suppl 2013;118:195–9. https://doi.org/10.1007/978-3-7091-1434-6_36.

23.Abdel Razek AAK, Talaat M, El-Serougy L, Abdelsalam M, Gaballa G. Differentiating Glioblastomas from Solitary Brain Metastases Using Arterial Spin Labeling Perfusion− and Diffusion Tensor Imaging−Derived Metrics. World Neurosurg 2019;127:e593–8. https://doi.org/10.1016/j.wneu.2019.03.213.

24.Uddin MdN, Figley TD, Solar KG, Shatil AS, Figley CR. Comparisons between multi-component myelin water fraction, T1w/T2w ratio, and diffusion tensor imaging measures in healthy human brain structures. Sci Rep 2019;9:2500. https://doi.org/10.1038/s41598-019-39199-x.

25.Sagawa H, Fushimi Y, Nakajima S, Fujimoto K, Miyake KK, Numamoto H, et al. Deep Learning-based Noise Reduction for Fast Volume Diffusion Tensor Imaging: Assessing the Noise Reduction Effect and Reliability of Diffusion Metrics. Magn Reson Med Sci MRMS Off J Jpn Soc Magn Reson Med 2020. https://doi.org/10.2463/mrms.tn.2020-0061.

26.Farrell JAD, Landman BA, Jones CK, Smith SA, Prince JL, van Zijl PCM, et al. Effects of SNR on the Accuracy and Reproducibility of DTI-derived Fractional Anisotropy, Mean Diffusivity, and Principal Eigenvector Measurements at 1.5T. J Magn Reson Imaging JMRI 2007;26:756–67. https://doi.org/10.1002/jmri.21053.

Author responsibilities, integrity, ethics

This is an **editable** PDF form. It should **be saved to your computer, then completed** using Adobe reader or equivalent. Please **do NOT substitute** any other document (text file, scanned image, etc.).

Article title : Deep learning-based noise reduction preserves quantitative biomarkers in patients with brain tumors

Human and animal rights

- [x] The authors declare that the work described has been carried out in accordance with the Declaration of Helsinki of the World Medical Association revised in 2013 for experiments involving humans as well as in accordance with the EU Directive 2010/63/EU for animal experiments.
- [ ] The authors declare that the work described has not involved experimentation on humans or animals.

Informed consent and patient details

- [ ] The authors declare that this report does not contain any personal information that could lead to the identification of the patient(s) and/or volunteers.
- [x] The authors declare that they obtained a written informed consent from the patients and/or volunteers included in the article and that this report does not contain any personal information that could lead to their identification.
- [ ] The authors declare that the work described does not involve patients or volunteers.

Disclosure of interest

- [x] The authors declare that they have no known competing financial or personal relationships that could be viewed as influencing the work reported in this paper.
- [ ] The authors declare the following financial or personal relationships that could be viewed as influencing the work reported in this paper:

Funding

- [ ] This work did not receive any grant from funding agencies in the public, commercial, or not-for-profit sectors.
- [x] This work has been supported by:

the FERCM (Fonds d'Études et de Recherche du Corps Médical)

Author contributions

☑ All authors attest that they meet the current International Committee of Medical Journal Editors (ICMJE) criteria for Authorship.

☐ All authors attest that they meet the current International Committee of Medical Journal Editors (ICMJE) criteria for Authorship. Individual author contributions are as follows:

Figure

Click here to access/download;Figure;Figures.docx

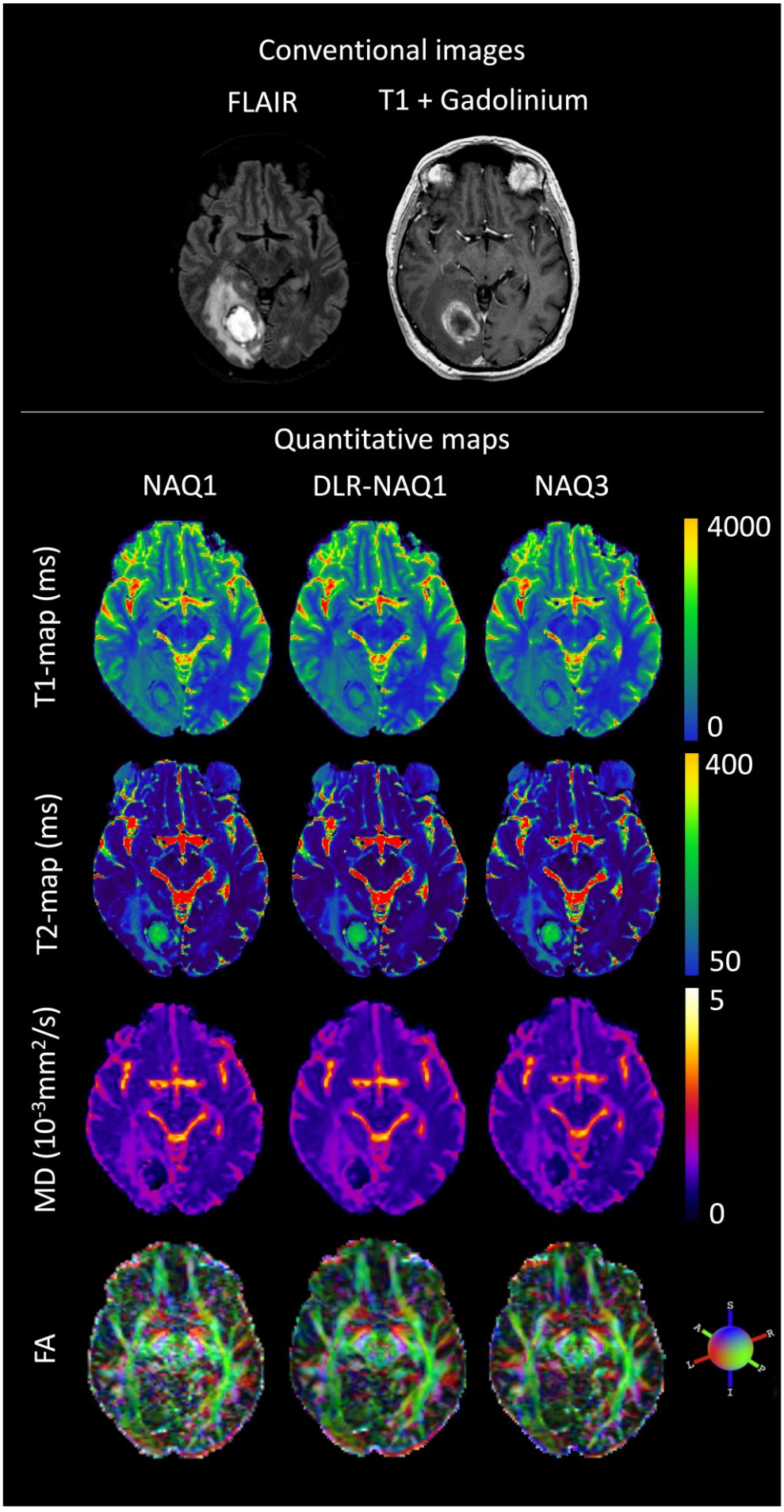

Fig. 1. 65-year-old male with a right occipito-parietal high-grade glioma. Top row: **Conventional sequences showing the enhancing portion of the tumor on T1-W after Gadolinium injection surrounded by peri-tumoral oedema and tumoral infiltration on FLAIR.** From top to bottom: representative T1, T2, MD and FA maps reconstructed from NAQ1, DLR-NAQ1 and NAQ3. **FA is displayed as diffusion encoded-color map.** DLR: denoising approach using Deep Learning Reconstruction; MD: Mean Diffusivity; **FA: Fractional Anisotropy.**

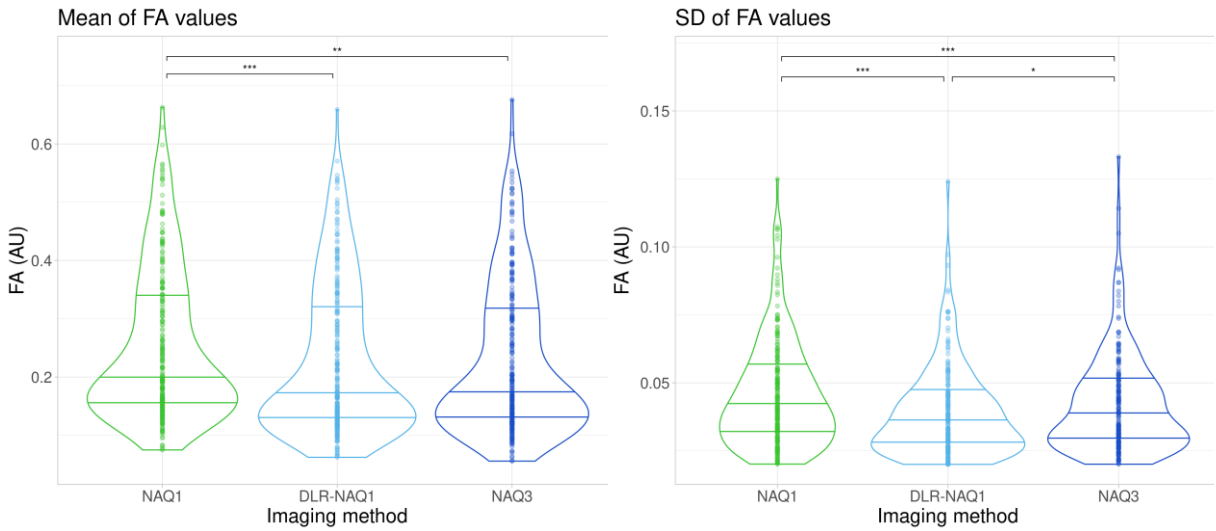

Fig. 2. Violin plots comparing FA across the different acquisition-reconstruction methods on pooled ROI locations. The Y-axis represents the mean FA (left panel) and the SDs (right panel) respectively. The middle, upper and lower horizontal bars represent respectively the median, lower and upper quartile. Note that the putamen ROI has been removed considering the significant interaction effect between the ROI location and acquisition-reconstruction methods for FA. AU: Arbitrary Units; DLR: denoising approach using Deep Learning Reconstruction; FA: Fractional Anisotropy; MD: Mean Diffusivity; NAQ: Number of Acquisitions; *p<0.05; **p<0.01; ***p<0.001.

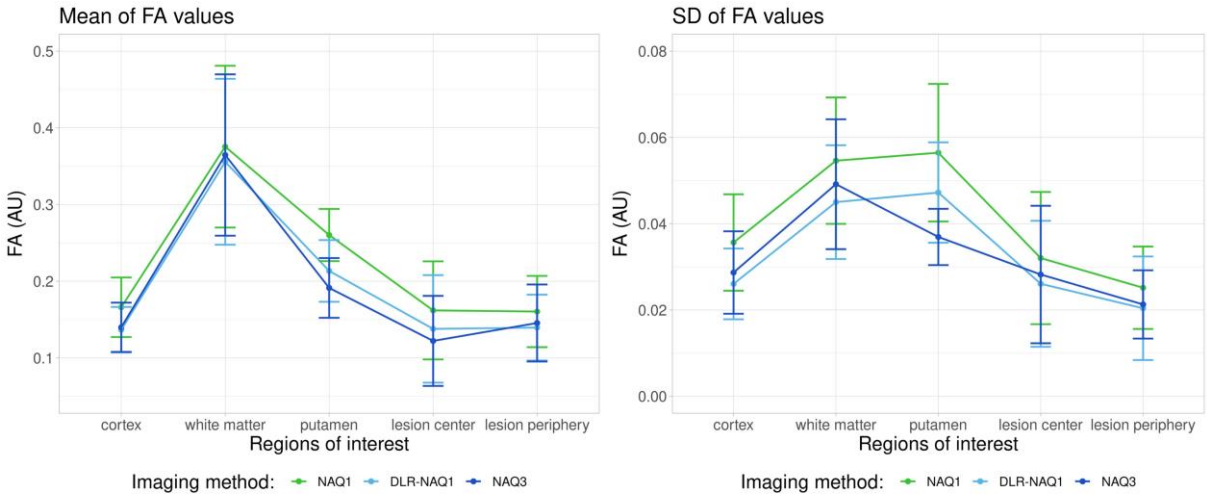

Fig. 3. Interaction plot for mean (a) and SD (b) of FA values, with respect to acquisition-reconstruction method and ROI location.

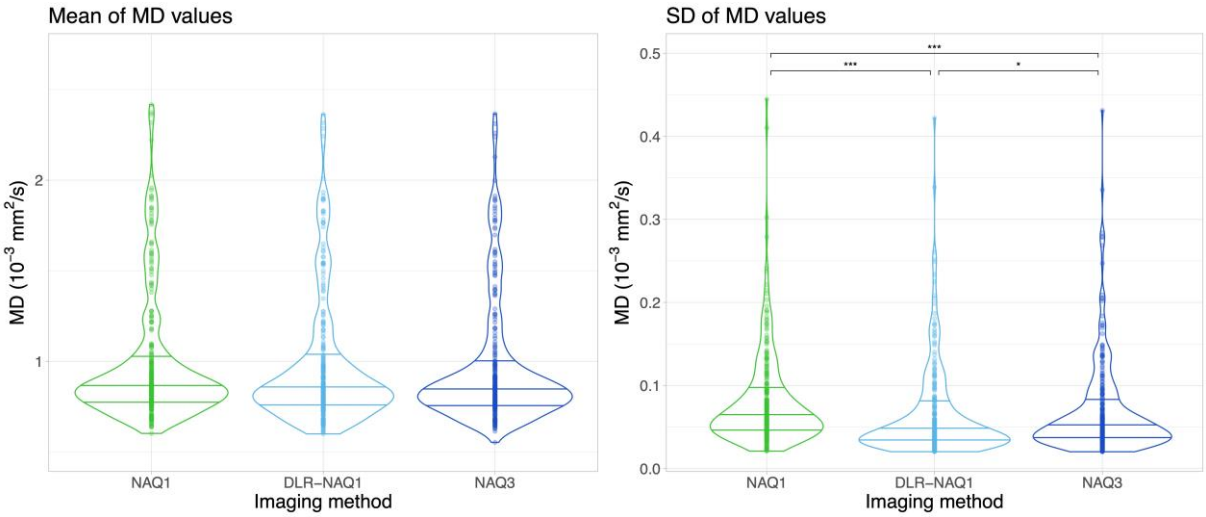

Fig. 4. Violin plots comparing MD values (x 10^{-3}mm^2/s) across the different acquisition-reconstruction methods on pooled ROI locations. The Y-axis represents the mean MD (left panel) and the SDs (right panel) respectively. The middle, upper and lower horizontal bars represent respectively the median, lower and upper quartile. DLR: denoising approach using Deep Learning Reconstruction; MD: Mean Diffusivity; NAQ: Number of Acquisitions; *p<0.05; ***p<0.001.

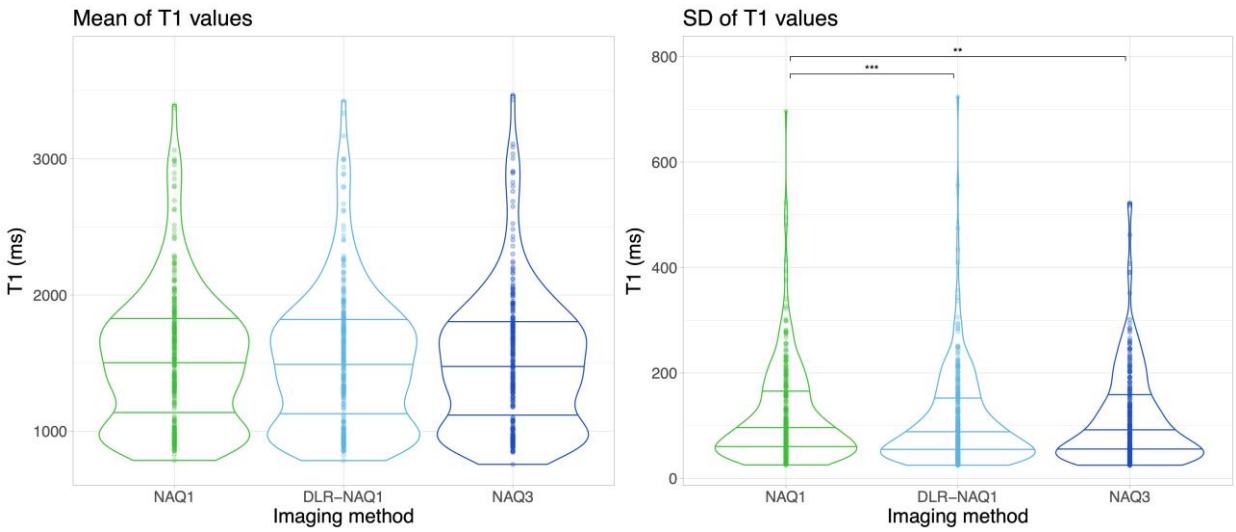

Fig. 5. Violin plots comparing T1 (ms) across the different acquisition-reconstruction methods on pooled ROI locations. The Y-axis represents the mean T1 (left panel) and the SDs (right panel) respectively. The middle, upper and lower horizontal bars represent respectively the median, lower and upper quartile. DLR: denoising approach using Deep Learning Reconstruction; NAQ: number of acquisitions; ** $p<0.01$; *** $p<0.001$.

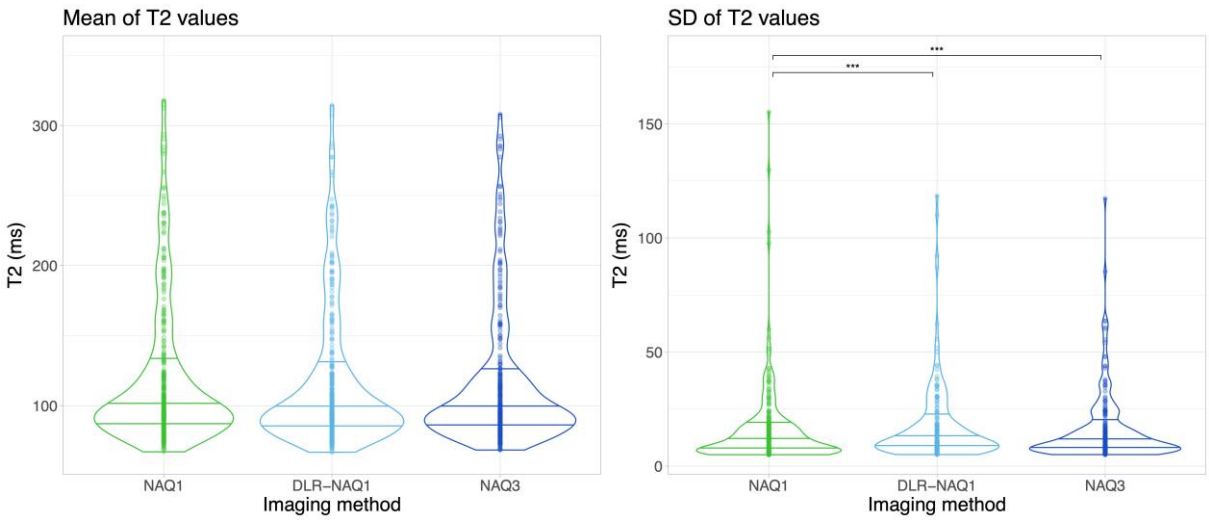

Fig. 6. Violin plots comparing T2 values (ms) across the different acquisition-reconstruction methods on pooled ROI locations. The Y-axis represents the mean T2 (left panel) and the SDs (right panel) respectively. The middle, upper and lower horizontal bars represent respectively the median, lower and upper quartile. DLR: denoising approach using Deep Learning Reconstruction; NAQ: number of acquisitions; ***p<0.001.

Table 1

Characteristics of the studied population.

Characteristics	Findings
Participants, number	22
Sex (male/female)	11 / 11
Age (years ± SD)	55.9 ± 14.1
Lesion type (number of patients)	
Metastasis	7
Lung cancer	**3**
Melanoma	**2**
Colorectal cancer	**1**
Breast cancer	**1**
High grade glioma	9
Low grade glioma	2
DNET	2
Lymphoma	1
Pseudo tumor	1

DNET: Dysembryoplastic Neuroepithelial Tumor; Pseudo tumor: toxoplasmosis

Table 2

MR acquisition and DLR parameters.

Parameters	MPRAGE	DTI	MP2RAGE	FSE
Related images	T1-WI	Diffusion	T1-RT maps	T2-RT maps
Acq. plane	3D	3D	3D	2D
Coverage	Whole brain	Whole brain	Tumor-centered	Tumor-centered
Image matrix	256×256	120×112	320×448	320×448
FOV (mm)	256×256	235×219	230×230	230×230
Slice thickness (mm)	1	2	2.5	2
Voxel size (mm)	1x1x1	01.95×1.95×2	0.71×0.51×2.5	0.71×0.51×2
Slice gap (mm)	0	0	0	0.5
Slices	160	70	29	29
TR (ms)	6.5	5207	7.5	6043
TE (ms)	3.0	85	3.3	20/60/100/140
TI (ms)	950	NA	664/3300	NA
Intershot (s)	2.5	NA	7	NA
Flip angle (degree)	9	90	8/9	90
b values (mm^2/s)	NA	0/1000	NA	NA
Diffusion directions (number)	NA	30	NA	NA
SPEEDER				
Phase encoding	1.8	2	2	2.5
Slice encoding	1.5	NA	1.4	NA
Multi-band	NA	2	NA	NA
Number of acq.	1	1/3	1/3	1/3

Scanning time				
NAQ1	5min 20sec	2min 58sec	3min 09sec	2min 44sec
NAQ3	NA	8min 52sec	9min 27sec	7min 58sec
DLR (on NAQ1)				
Denoising level	**NA**	**9**	**1.5**	**9**
Blending factor	**NA**	**0.3**	**0**	**0.5**

DLR: denoising approach using Deep Learning Reconstruction; DTI: Diffusion Tensor Imaging; FOV: Field Of View; FSE: T2-Fast Spin Echo; MPRAGE: T1-Magnetization Prepared Rapid Acquisition Gradient Echoes; MP2RAGE: T1-Magnetization Prepared 2 Rapid Acquisition Gradient Echoes; Multi-band: simultaneous multi-slice imaging; NA: Not Applicable; RT: Relaxation Time; TE: Echo Time; TI: Inversion Time; TR: Repetition Time; SPEEDER: acceleration factors of in-plane parallel imaging; WI: Weighted-Images.

Table 3

Structural Similarity Index (SSIM) values using NAQ3 as a reference (median ± MAD) and results of Wilcoxon signed rank test.

Parameter maps	NAQ1	NAQ1-DLR	P-value*
T1-RT	0.927 ± 0.055	0.932 ± 0.048	0.03
T2-RT	0.924 ± 0.025	0.938 ± 0.019	$4.77\ 10^{-7}$
FA	0.764 ± 0.033	0.772 ± 0.026	0.01
MD	0.908 ± 0.021	0.920 ± 0.015	$4.77\ 10^{-7}$

*Wilcoxon signed rank test

DLR: denoising approach using Deep Learning Reconstruction; FA: Fractional Anisotropy; MD: Mean Diffusivity; NAQ: number of acquisitions; T1-RT: T1-Relaxation Time; T2-RT: T2-Relaxation Time

Table 4

Mean and SD values of each parameter across the different acquisition-reconstruction methods.

Variables	Mean			SD		
Acq. Reconstruction	NAQ1	DLR-NAQ1	NAQ3	NAQ1	DLR-NAQ1	NAQ3
FA (excluding Putamen)	0.199 ± 0.095	0.171 ± 0.089	0.175 ± 0.097	0.038 ± 0.019	0.030 ± 0.015	0.032 ± 0.018
FA (in the Putamen)	0.260 ± 0.034	0.213 ± 0.040	0.191 ± 0.039	0.057 ± 0.016	0.047 ± 0.012	0.037 ± 0.007
MD	0.862 ± 0.152	0.847 ± 0.166	0.847 ± 0.147	0.061 ± 0.030	0.041 ± 0.023	0.048 ± 0.025
T1-RT	1484 ± 555	1467 ± 550	1462 ± 536	85.2 ± 60.6	74.6 ± 53.7	74.3 ± 61.3
T2-RT	98.1 ± 4.5	95.7 ± 24.0	96.5 ± 23.4	8.27 ± 5.14	5.71 ± 4.50	6.59 ± 4.34

Results are presented as median ± MAD. FA is analyzed separately in the putamen ROI due to the interaction effect between ROI and acquisition-reconstruction methods. FA is expressed in Arbitrary Units (AU); MD is expressed in $10^{-3}mm^2/s$; T1-RT and T2-RT are expressed in ms; DLR: denoising approach using Deep Learning Reconstruction; FA: Fractional Anisotropy; MD: Mean Diffusivity; NAQ: number of acquisitions; T1-RT: T1-Relaxation Time; T2-RT: T2-Relaxation Time